TU Delft

Delft University of Technology

Document Version
Final published version

Licence
CC BY

Citation (APA)
Li, B., Basu, S., Watson, S. J., & Russchenberg, H. W. J. (2021). Mesoscale modeling of a “Dunkelflaute” event. *Wind Energy*, *24*(1), 5-23. https://doi.org/10.1002/we.2554

Important note
To cite this publication, please use the final published version (if applicable).
Please check the document version above.

Copyright
In case the licence states “Dutch Copyright Act (Article 25fa)”, this publication was made available Green Open Access via the TU Delft Institutional Repository pursuant to Dutch Copyright Act (Article 25fa, the Taverne amendment). This provision does not affect copyright ownership.
Unless copyright is transferred by contract or statute, it remains with the copyright holder.

Sharing and reuse
Other than for strictly personal use, it is not permitted to download, forward or distribute the text or part of it, without the consent of the author(s) and/or copyright holder(s), unless the work is under an open content license such as Creative Commons.

Takedown policy
Please contact us and provide details if you believe this document breaches copyrights.
We will remove access to the work immediately and investigate your claim.

This work is downloaded from Delft University of Technology.

Received: 9 March 2020 | Revised: 22 June 2020 | Accepted: 2 July 2020

DOI: 10.1002/we.2554

Check for updates

WILEY

RESEARCH ARTICLE

Mesoscale modeling of a "Dunkelflaute" event

Bowen Li[1] | Sukanta Basu[1] | Simon J. Watson[2] | Herman W. J. Russchenberg[1]

[1]Faculty of Civil Engineering and Geosciences, Delft University of Technology, Delft, The Netherlands

[2]Faculty of Aerospace Engineering, Delft University of Technology, Delft, The Netherlands

Correspondence
Sukanta Basu, Faculty of Civil Engineering and Geosciences, Delft University of Technology, Stevinweg 1, 2628 CN Delft, The Netherlands.
s.basu@tudelft.nl

Abstract

In the near future, wind and solar generation are projected to play an increasingly important role in Europe's energy sector. With such fast-growing renewable energy development, the presence of simultaneous calm wind and overcast conditions could cause significant shortfalls in production with potentially serious consequences for system operators. Such events are sometimes dubbed "Dunkelflaute" events and have occurred several times in recent history. The capabilities of contemporary mesoscale models to reliably simulate and/or forecast a Dunkelflaute event are not known in the literature. In this paper, a Dunkelflaute event near the coast of Belgium is simulated utilizing the Weather Research and Forecasting (WRF) model. Comprehensive validation using measured power production data and diverse sets of meteorological data (e.g., floating lidars, radiosondes, and weather stations) indicates the potential of WRF to reproduce and forecast the boundary layer evolution during the event. Extensive sensitivity experiments with respect to grid-size, wind farm parameterization, and forcing datasets provide further insights on the reliability of the WRF model in capturing the Dunkelflaute event.

KEYWORDS

North Sea, power reliability, solar energy, wake parameterization, wind energy

1 | INTRODUCTION

Under various energy transition scenarios, a rapid growth in renewable energy generation can be foreseen, leading to a more sustainable energy system in Europe. In order to fulfill the target of 40% greenhouse gas emission reduction by 2030 (compared to the emission level of 1990), it is projected that a significant share (~ 32%) of the total energy consumption in Europe will be from renewable sources by 2030.[1] This share could be as high as ~ 66% by 2050.[2] In order to meet these ambitious targets, the North Sea region will play an increasingly important role. By the year 2045, an offshore wind energy installation of around 180 GW in the region is expected.[3] Belgium's massive investment in the renewable energy sector, including offshore wind farms over the North Sea, indicates that a complete shut-down of nuclear power plants by 2025 is attainable.[4] As far as the Netherlands is concerned, the roll-out of offshore wind farms is anticipated to expand at a rate of 1 GW per year up until 2030.[5] By 2050, an aggregated 75 GW installation of offshore wind farms is planned.

Unlike fossil fuel-based energy sources, some of the renewable energy sources (especially, wind and solar) strongly rely on meteorological conditions. As such sources of energy play a larger role in electricity networks, this presents an increasing challenge in terms of balancing supply and demand. Therefore, it is important to increase our understanding and forecasting capability of certain weather phenomena which can result in adverse renewable energy production from a system operator perspective. Such advanced knowledge and tools will further support the continuing growth of renewables in the foreseeable future.

This is an open access article under the terms of the Creative Commons Attribution License, which permits use, distribution and reproduction in any medium, provided the original work is properly cited.
© 2020 The Authors. Wind Energy published by John Wiley & Sons Ltd

In this paper, we focus on one such weather phenomenon called "Dunkelflaute" as it is rapidly becoming a major concern for the renewable energy community.[6] The word Dunkelflaute was coined by combining two German words "Dunkelheit" (darkness) and "Windflaute" (little wind) to describe heavy overcast skies and weak wind conditions. These meteorological events can last from a few hours to a few consecutive days. It is needless to say that under the influence of such a meteorological condition, little or no wind and solar energy can be produced.

On the 30th April 2018, an unexpected Dunkelflaute event occurred over the southern part of the North Sea and caused a large imbalance in renewable power generation and overall consumption. Given the acuteness of the situation, TenneT—the main transmission system operator for Germany and the Netherlands—had to issue an emergency alert in the Netherlands.[7,8] The crisis could not be avoided by simple load management or by making use of reserve power; instead, a substantial amount of electricity had to be imported from neighboring countries at high market price.

This Dunkelflaute event was not an isolated episode. As a matter of fact, over the past few years, several Dunkelflaute events occurred in Belgium,[9-12] Germany,[6,13-15] and other neighboring countries. Some of them caused significant impacts on the power grids and electricity markets. There is no reason to believe that the occurrences of Dunkelflaute will subside in the future. Instead, with the ever increasing penetration of renewables in the power grid, the (negative) impacts of Dunkelflaute events will likely become more and more detrimental.

As a first step towards better forecasting of Dunkelflaute events, in this study, we investigate a recent Dunkelflaute event which occurred in Belgium. We analyze a diverse suite of observational datasets for detailed characterization. We evaluate the performance of a state-of-the-art mesoscale model, called the Weather Research and Forecasting (WRF) model,[16,17] in capturing this event. The organization of this paper is as follows. In Section 2, we briefly provide the meteorological background of the Dunkelflaute phenomenon. The selected case study is discussed in Section 3. The observational datasets and our atmospheric modeling framework are described in Sections 4 and 5, respectively. The simulated results along with in-depth analysis are documented in Section 6. At the end, we summarize our findings and elaborate on potential future research in this arena. A brief climatology of Dunkelflaute events in Belgium is documented in Appendix A.

2 | DUNKELFLAUTE: A METEOROLOGICAL PERSPECTIVE

The word Dunkelflaute does not exist in the vocabulary of meteorologists. Instead, they commonly refer to this phenomenon as the "anticyclonic gloom."[18,19] There are also localized names to describe this dull and drab weather phenomenon. For example, in the dialect of Lincolnshire, UK, it is known as *moäky* or *moke*.[20]

One of the earliest references to anticyclonic gloom can be found in a sublime article by Captain C. K. M. Douglas.[21] Exactly 100 years ago, he conducted a comprehensive study on cloud characterization using aerial photography and stated:

> "It is not generally realised that when the sky is covered with a gloomy canopy of cloud, with the inevitable smoky haze over towns and for a considerable distance to leeward, one has only to ascend about a mile in order to enter a region with clear blue sky above, and a sea of white billowy cloud underneath, which stretches in all directions to a distant horizon which stands out sharply owing to the perfect visibility.
>
> …
>
> In winter the sky is very frequently overcast with a single sheet of low cloud varying in thickness from 500 to 2000 feet. This type of cloud is very characteristic of anticyclonic weather. There may be several days or a week of overcast sky, a state of affairs described by Mr. W. H. Dines as anticyclonic gloom."

Over the years, our overall understanding of anticyclonic gloom has been steadily increasing. We now know that it is characterized by a high pressure system, extensive stratus and/or stratocumulus cloud cover, strong subsidence inversion, near-calm wind, low surface temperature, and possibly foggy nights.[22,23] We are also aware of the fact that anticyclonic gloom is predominantly a winter-time phenomenon. Although, it can happen during the summer months under appropriate synoptic meteorological conditions and sea state, for example, Galvin.[24]

In spite of basic characterizations, more detailed knowledge (e.g., radiation and heat budgets, dynamical evolution, and dissipation) pertaining to anticyclonic gloom is severely lacking in the atmospheric science literature. For example, after the (inconclusive) studies by Priestley and Swinbank[25] and Robinson[26] around 1950, we have not come across any follow-up publication on heat budgets of anticyclonic gloom. In the era of advanced instrumentation (including remote-sensing) and cutting-edge numerical modeling (e.g., large-eddy simulation), such a critical knowledge-gap should not exist.

In this context, it is important to note that there have been several comprehensive modeling studies[27-29] probing both stratus- and stratocumulus-topped boundary layers. However, to the best of our knowledge, none of these studies focused on the weak wind (or calm) regime – a necessary ingredient for the genesis of anticyclonic gloom. It is the sole purpose of the present study to investigate this specific regime using the WRF model.

3 | DESCRIPTION OF CASE STUDY

In January 2017, Belgium experienced a total of nine days of Dunkelflaute (anticyclonic gloom).[9-12] During these days, due to gentle breeze and overcast conditions, the energy production from wind and solar farms was far below their rated values. To further aggravate the situation, a nuclear power plant malfunctioned at the same time. Several measures, including more electricity generation from natural gas, additional power imports from neighboring countries, and other flexibility options, were undertaken to handle this acute problem.[30] Modeling by Elia of a similar extended period of low renewable energy generation (wind and PV) under a future 2040 scenario indicated that there could be an overall shortage of more than 1000 GWh of energy[10] which would be difficult to fill with existing storage technology.

The aggregated wind (onshore and offshore) and solar power production data for Belgium are publicly available from Elia (https://www.elia.be)—the transmission system operator in Belgium. The production data for the month of January 2017 are shown Figure 1. In lieu of any objective (quantitative) criterion in the literature, here, we define a period as Dunkelflaute when onshore wind, offshore wind, and solar power generation all fall below 10% of their respective nominal capacities. These periods are marked as lightly shaded gray regions in Figure 1. The weak wind conditions, occurring during nighttime hours (no solar power generation), are demarcated by a darker shade. In this paper, we focus on two of these Dunkelflaute periods: January 15–17 and January 22–25.

The surface analyses for January 15th and January 25th are shown on the top panel of Figure 2. It is clear that the Azores high was present in the eastern Atlantic on January 15th. At the same time, over the North Sea region, the gradients of surface pressure were relatively strong and were conducive to adequate wind power generation (see top-panel of Figure 1). In the following days, a stronger anticyclone (high pressure center) developed over continental Europe and moved slowly eastward. At its peak, it reached an impressive magnitude of 1042 hPa (not shown). On and around January 25th, the anticyclone was located over Germany. Given the vast expanse of the high pressure regions (refer to top-right panel of Figure 2), the pressure gradients were rather slack and led to extremely calm wind conditions. It is needless to say that neither the onshore nor the offshore wind farms in Belgium produced any energy on that day.

During both Dunkelflaute events of January 15th–17th and January 22nd–25th, the southern part of the North Sea was overcast with thick clouds (bottom panels of Figure 2), resulting in very little solar radiation reaching the surface. As shown in the bottom panel of Figure 1, the solar energy production was virtually negligible during these Dunkelflaute periods.

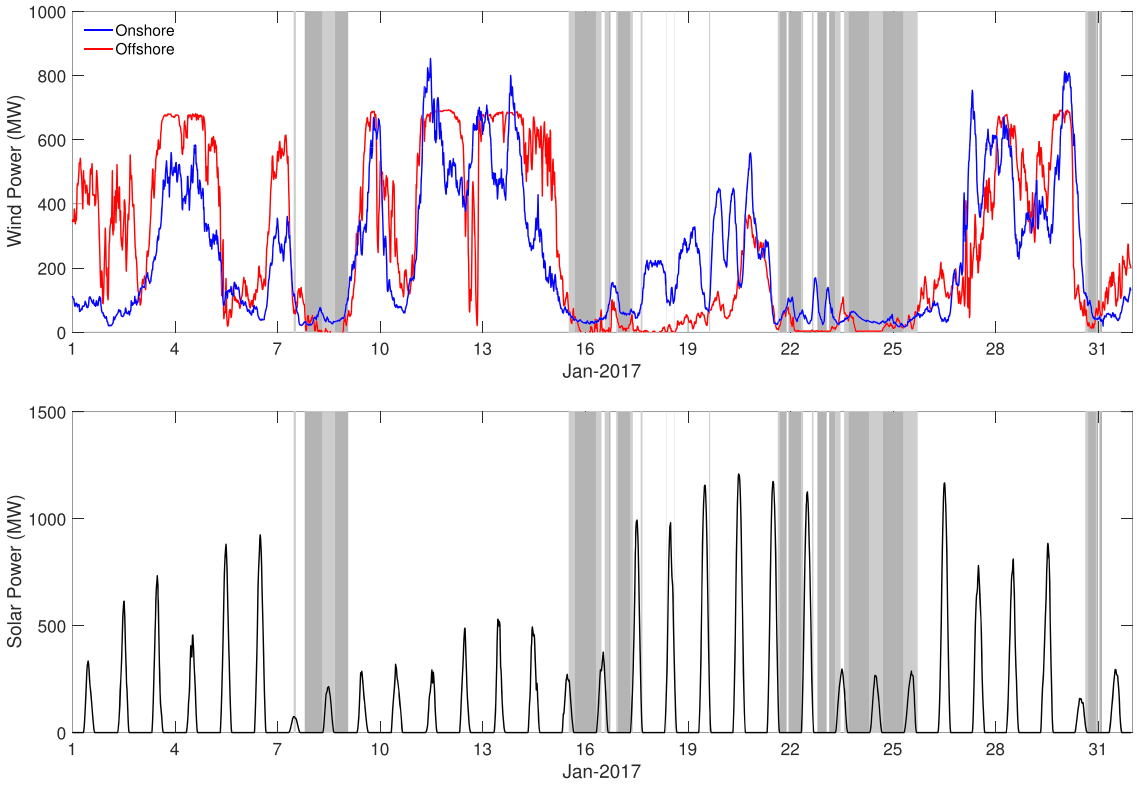


FIGURE 1 Time series of wind energy (top panel) and solar energy (bottom panel) production during January 2017 (data source: Elia.be). The daytime Dunkelflaute periods are represented with lightly shaded gray regions. The weak wind conditions, occurring during nighttime hours (no solar power generation), are demarcated by a darker shade. If two gray regions are separated by no more than one hour, they have been merged together [Colour figure can be viewed at wileyonlinelibrary.com]

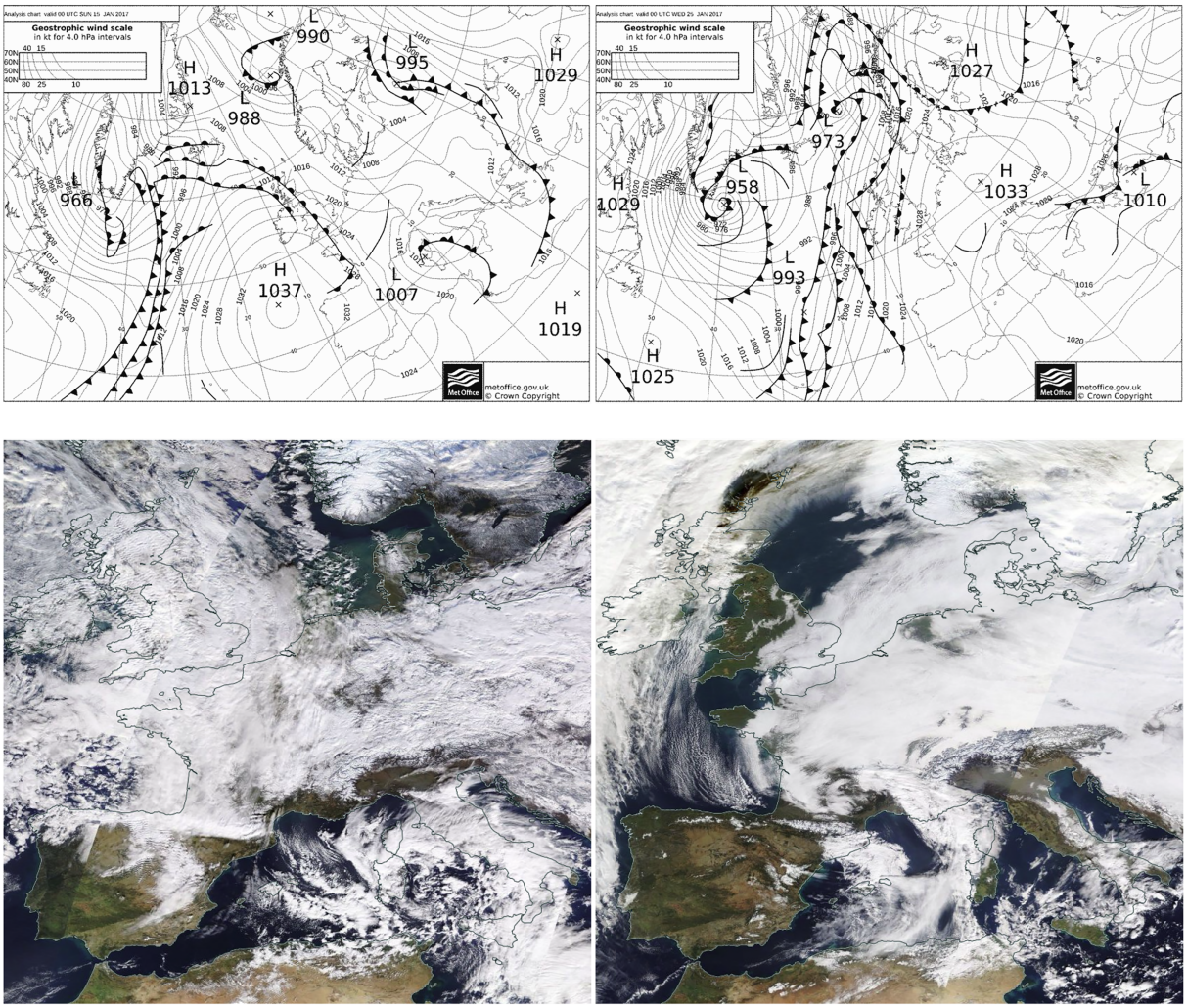


FIGURE 2 Synoptic weather maps for January 15th (top-left panel) and January 25th (top-right panel) of 2017. Source: https://www.wetterzentrale.de/. MODIS satellite-based reflectance maps for January 15th (bottom-left panel) and January 25th (bottom-right panel) of 2017. Source: https://worldview.earthdata.nasa.gov [Colour figure can be viewed at wileyonlinelibrary.com]

Even though it is completely out of the scope of the present study, we would like to point out that the atmospheric circulation patterns over continental Europe were very unusual during January 2017 (refer to Appendix B). They caused extreme cold and violent storms at various places resulting in numerous deaths.[31] From that perspective, these Dunkelflaute events were far less sinister in nature.

4 | DESCRIPTION OF OBSERVATIONAL DATASETS

During January 2017, Belgium had only three operational offshore wind farms, C-Power, Northwind, and Belwind I, with a combined capacity of 712 MW. These wind farms and their associated wakes can be seen in the left panel of Figure 3. In this paper, we have used aggregated power production data from these wind farms in conjunction with solar farms to characterize the Dunkelflaute phenomenon. The temporal granularity of these datasets is 15 min. Note that these data have been post-processed by Elia to account for missing data or other data anomalies.[33,34]

In addition to the power production data, we use meteorological data from several offshore and onshore locations. First of all, we make use of several lidar-based wind datasets which are publicly available via TNO (fomerly ECN, the Energy Research Center of the Netherlands). Floating lidars (middle panel of Figure 3), as well as lidars on fixed platforms (right panel of Figure 3) were utilized to collect wind data. At Borssele Wind Farm Zone (BWFZ) and Hollandse Kust Zuid (HKZ), SEAWATCH floating lidar systems (equipped with ZX, formerly ZephIR, 300S lidars) were deployed by Fugro. These lidars provided wind profiling data for 10 heights between 30 and 200 m above mean sea level (MSL). The temporal resolution of all the wind time-series is 10 min.

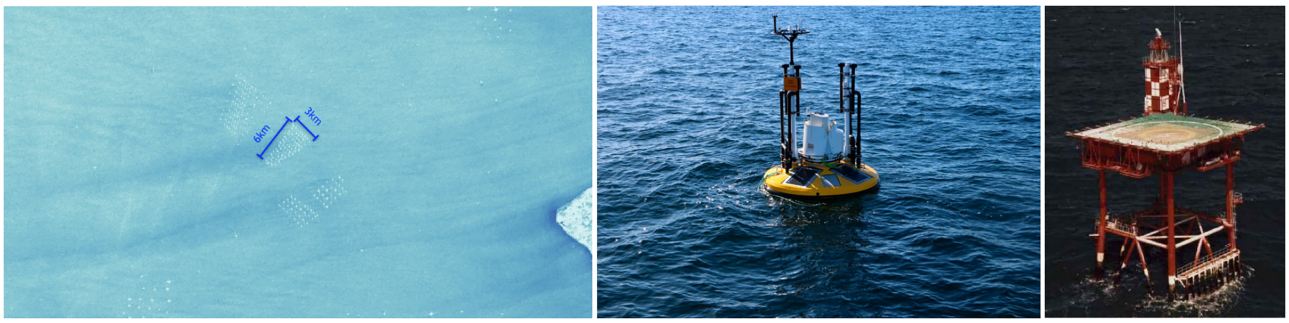


FIGURE 3 Left panel: synthetic aperture radar (SAR) image of Belgian offshore wind farms (source: Google Earth Engine); middle panel: image of the SEAWATCH wind lidar buoy located at Borssele Wind Farm Zone (BWFZ, source: BWFZ Project and Site Description); right panel: image of Lichteiland Goeree (LEG, source: DNV-GL[32]) [Colour figure can be viewed at wileyonlinelibrary.com]

The wind dataset from BWFZ has only a handful of missing samples. These measurements were validated against a cup-anemometer at Vlakte van de Raan wind station and were found to be of high quality.[35,36] In the HKZ region, two floating lidars were taking wind measurements at locations called HKZA and HKZB. Unfortunately, due to intermittent transmission failures, the wind dataset from HKZA has several gaps. The lidar at HKZB did not suffer from a similar data-loss problem. In fact, the wind data at HKZB were strongly correlated with conventional anemometer-based data from Lichteiland Goeree (LEG) and EuroPlatform (EPL) stations attesting to its high quality.[37,38] At LEG and EPL platforms, ZX wind lidars were also deployed and measured at several heights (from 90 to 315 m) every 10 min.[39,40] The locations of BWFZ, HKZ, LEG, EPL, and the offshore wind farms can be seen in the left panel of Figure 4.

Next, measurements from the Stabroek automated weather station (AWS) are utilized in this study. This AWS is operated by the Royal Meteorological Institute (RMI) of Belgium, and its location can be seen in the left panel of Figure 4. The recorded shortwave radiation data have a temporal resolution of 10 min.[41]

Lastly, sounding datasets from three land-based stations (Herstmonceux, Norderney, and EDZE Essen, locations shown in the right panel of Figure 4), are utilized for the characterization of the vertical structure of the atmosphere during the Dunkelflaute periods. These datasets are provided by the University of Wyoming[42] and contain vertical profiles of wind speed, potential temperature, and several other meteorological variables.

5 | MODEL SETUP

The Weather Research and Forecasting (WRF) model (version 3.9.1.1) is employed here to simulate the atmospheric conditions associated with the aforementioned Dunkelflaute event. A total of six different simulations are performed by varying large-scale forcing data and physical

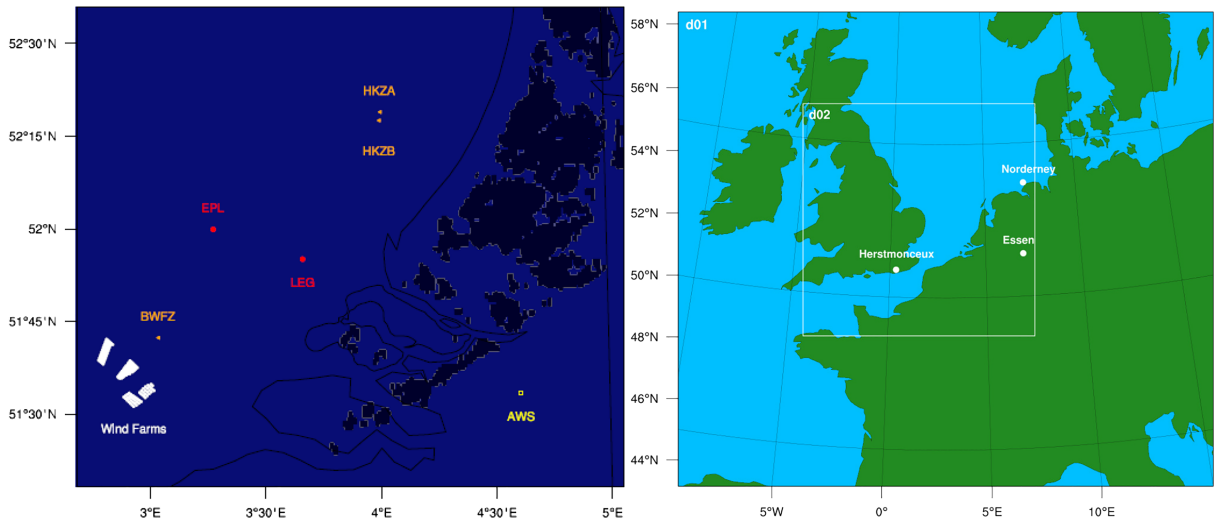


FIGURE 4 Left panel: locations of the Belgian offshore wind farms and the meteorological stations. Right panel: domain configuration for the WRF simulations when the ERA5 reanalysis dataset is used for initial and boundary conditions. The locations of the radiosonde launch locations are overlaid on this plot [Colour figure can be viewed at wileyonlinelibrary.com]

TABLE 1 Technical details of the WRF simulations.

WRF Run	IC/BC	Grid Size, km	Time Step, s	PBL Scheme	Wind Farm Scheme	Grid Nudging	Initialization Date
WRF–ERA5	ERA5	9/3	45/15	MYNN 2.5 level	on	on	Jan 14, 2017
WRF–ERA5*	ERA5	9/3	45/15	MYNN 2.5 level	off	on	Jan 14, 2017
WRF–ERA5#	ERA5	9/3	45/15	YSU	off	off	Jan 14, 2017
WRF–ERA-I	ERA-Interim	27/9/3	90/45/15	MYNN 2.5 level	on	on	Jan 14, 2017
WRF–GFS	GFS operational	27/9/3	90/45/15	MYNN 2.5 level	on	on	Jan 14, 2017
WRF–GFS+	GFS operational	27/9/3	90/45/15	MYNN 2.5 level	on	on	Jan 21, 2017

parameterizations; see Table 1 for details. The first five simulations start at 00 UTC on January 14, 2017, and last for a total of 14 days. The last simulation (called WRF−GFS+) is initialized at 00 UTC of January 21st. Model output are saved every 10 min.

All the simulations utilize 51 vertical levels with non-uniform grid spacing with the top of the model reaching approximately 16 km from the surface. The lowest grid level is approximately at 8 m from the surface, and there are 18 levels in the lowest 1 km of the model atmosphere. In every simulation (with one exception), grid nudging is applied above approximately 2 km in order to keep the simulations in sync with the large-scale forcing data. In addition, the sea-surface temperature field is continuously updated throughout the simulations.

Numerous physical parameterization options are available in the WRF model to represent turbulence, land-atmosphere interactions, radiation, cloud microphysics, and other processes. Based on our past experience, we have used the following parameterizations: NOAH land surface model,[43] Rapid Radiative Transfer Model for Global Climate Models (RRTMG) for longwave radiation and shortwave radiation,[44] WRF Single-Moment 5-class microphysics scheme,[45] and Kain-Fritsch cumulus scheme[46] (only activated for grid sizes coarser than 5 km). We have selected the Mellor-Yamada-Nakanishi-Niino (MYNN) 2.5 level scheme[47] as the default planetary boundary layer (PBL) parameterization. However, in one of the WRF runs, we use the Yonsei University (YSU) scheme[48,49] to investigate the sensitivity of the simulated results with respect to PBL parameterizations.

The wind farm parameterization by Fitch et al[50] is activated in four of the WRF runs to simulate the effects of the Belgian offshore wind turbines on the atmospheric flow fields. The effects of the wind turbines are represented as a drag-induced energy sink and increased turbulence in the vertical levels containing the rotor disk. The Fitch parameterization assumes that a fraction of the total energy flowing through the wind farm is used for power production (based on the turbine power coefficient), and the rest is converted into turbulent kinetic energy (determined by the turbine thrust coefficient). The simulated wind farm area consists of three Belgian offshore wind farms: C-Power, Northwind, and Belwind I. In the left panel of Figure 4, they are depicted as white polygons. There are a total of 182 wind turbines of five different types (Table 2). The power and thrust curves of these turbines are described in Appendix C.

Three different large-scale forcing datasets are used for initial conditions (IC) and boundary conditions (BC). The ERA5 reanalysis dataset (horizontal grid size: ∼31 km; sampling rate: 1 hourly) is available from 1979 to present day from the European Centre for Medium-Range Weather Forecasts (ECMWF).[51] The ERA-Interim reanalysis dataset (horizontal grid size: ∼79 km; sampling rate: 6 hourly) is also available from ECMWF.[52] In addition to these reanalysis datasets, we also use an operational forecast dataset (horizontal grid size: 0.25°; sampling rate: 3 hourly for 0 to 240-h period and 12 hourly for 240 to 384-h) from the Global Forecast System (GFS) to investigate if the Dunkelflaute periods could have been predicted in a real-time forecast scenario. The WRF−GFS and WRF−GFS+ simulations are initialized on January 14th and 21st, respectively, to investigate the impacts of prediction horizons on Dunkelflaute forecasting.

For the WRF runs involving ERA5, two nested domains are used (right panel of Figure 4). These domains are coupled in a one-way nesting mode. The outermost domain (d01) has a grid size of 9 km (domain size: 1890 km × 1674 km); whereas, the inner domain (d02) employs a grid size of 3 km (domain size: 819 km × 819 km). Given the coarser spatial resolution of the ERA-Interim and the GFS datasets, we deemed it necessary to use a three domain configuration. The largest domain (d01) for these runs uses a grid size of 27 km (domain size: 2673 km × 2943 km); it is not shown. The second domain (d02) and the third domain (d03) use grid sizes of 9 and 3 km, respectively. Their corresponding domain sizes exactly match the ones shown in the right panel of Figure 4.

TABLE 2 Information on the three Belgian offshore wind farms used in this study.

Wind Farm	Nameplate Capacity, MW	Turbines	Hub Height, m	Rotor Diameter, m
C-Power	325	6 Senvion 5 MW; 48 Senvion 6.2 MW	94	126
Northwind	216	72 Vestas V112 3 MW	71	112
Belwind I	171	55 Vestas V90 3 MW; 1 Alstom 6 MW	72	90

6 | RESULTS

In this section, we compare the WRF model-based simulated results against various observational data. In addition, we investigate the sensitivities of the simulated results with respect to grid-size, IC/BC, and wind farm parameterization.

6.1 | Time series analysis

Measured wind speed time-series for the period of 14th–28th of January 2017 are shown in the top panel of Figure 5. It is evident that the wind speeds were mostly lower than 5 m s^{-1} during the Dunkelflaute periods. More interestingly, wind speed shears within the layer of 40–180 m were virtually absent for almost the entire two-week period; thus, it can be inferred that the lower part of the boundary layer was well-mixed. Starting January 27th, we do see some signatures of wind speed shear in the measurements.

Measured wind speed time-series from four stations (i.e., LEG, EPL, BWFZ, and HKZ) over the North Sea are intercompared in the top-right panel of Figure 5. The selected measurement heights are close to the hub height of a Senvion 5 MW turbine (94 m). Specifically, at LEG and EPL, the selected measurement heights were at 91 m; whereas, at BWFZ and HKZ, they were at 100 m. As illustrated by Figure 5, the overall consensus of all the wind speed time-series is very high. Because these four stations are spread over a large area (see the left panel of Figure 4), it is safe to deduce that the wind speeds during the chosen time-period were spatially rather homogeneous.

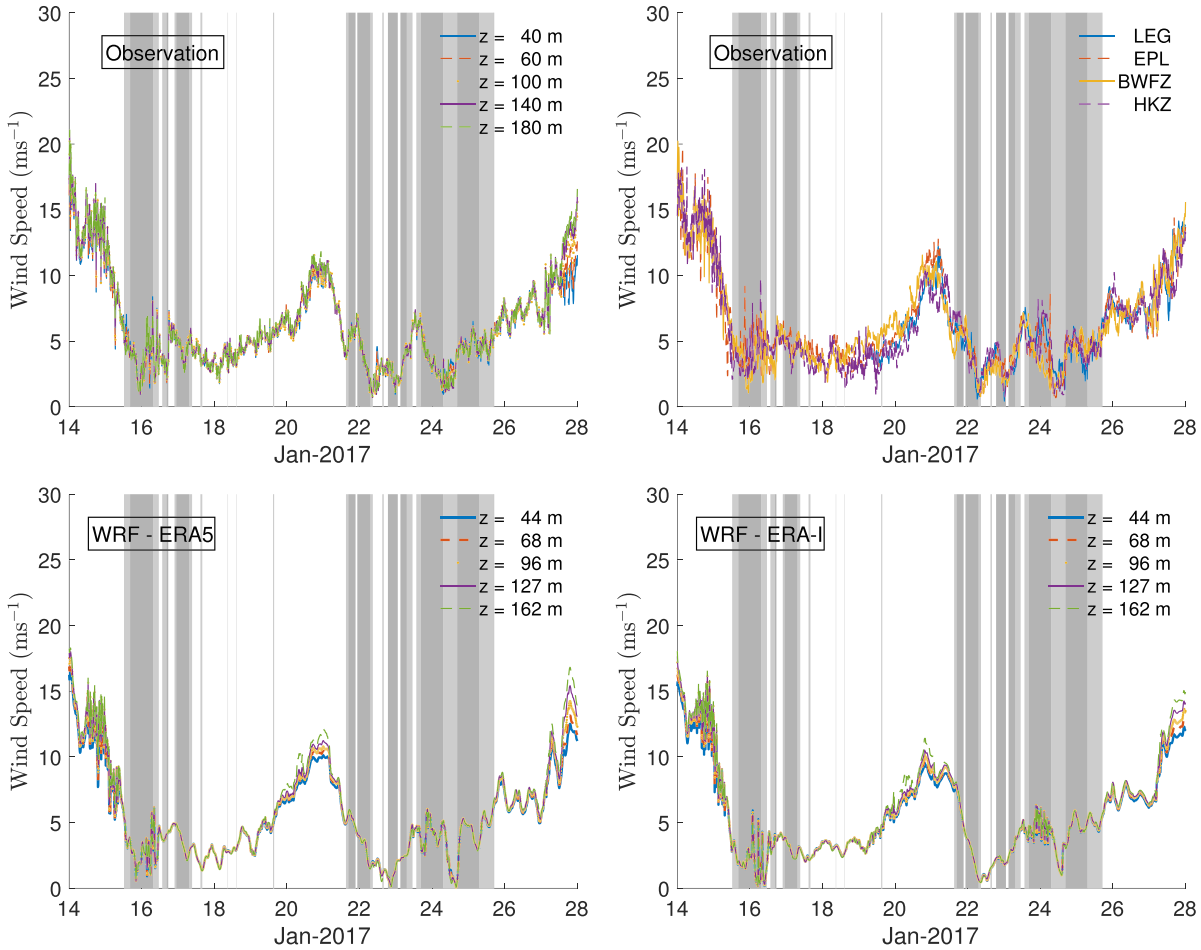


FIGURE 5 Top-left panel: wind speed time series from various heights measured at the BWFZ station. Top-right panel: hub height (∼91–100 m) wind speed time series measured at four locations over the North Sea (i.e., LEG, EPL, BWFZ, and HKZ). Simulated wind speed time series from various heights extracted from the WRF-ERA5 and WRF-ERA-I runs are shown in the bottom-left and bottom-right panels, respectively. Only the simulated data from the innermost domains (i.e., grid size of 3 km) are shown. The selected grid points are in close proximity to the BWFZ station. The daytime Dunkelflaute periods are represented with lightly shaded gray regions. The weak wind conditions, occurring during nighttime hours (no solar power generation), are demarcated by a darker shade [Colour figure can be viewed at wileyonlinelibrary.com]

The simulated wind speed time-series from the WRF–ERA5 and WRF-ERA-I runs are shown in the bottom panel of Figure 5. The selected grid points are close to the BWFZ station. Output from both the runs show similar temporal evolution patterns and strongly agree with the measured data in terms of magnitudes of both wind speeds and wind shears. On January 21st, the simulated data exhibited a small level of shear which were not present in the measurements.

As illustrated by Figure 6, the observed and simulated wind direction time-series varied a lot during January 14th–28th. The WRF–ERA5 run has more-or-less captured the overall trend. Some deviations are however noticeable.

In the left panel of Figure 7, the WRF model-generated wind power production data are overlaid on top of the measured data by Elia. It is clear that the wind farm parameterization of the WRF model is able to accurately capture the magnitudes of the power production including the rapid ramp-down and ramp-up events. During the Dunkelflaute periods, the measured power production data had a few sporadic episodes of power generation; the simulated data were unable to capture such traits.

Given the spatiotemporally intermittent cloud patterns (see the bottom panel of Figure 2), rigorous validation of the WRF model-generated radiation data is a challenging task. As a poor man's choice, we have decided to compare the simulated (downwelling) shortwave radiation data against the observational data from the Stabroek station. From the right panel of Figure 7, it is clear that the WRF model significantly overestimated the magnitudes of shortwave radiation during the Dunkelflaute periods; in other words, the cloudiness was weaker in the model than in the reality.

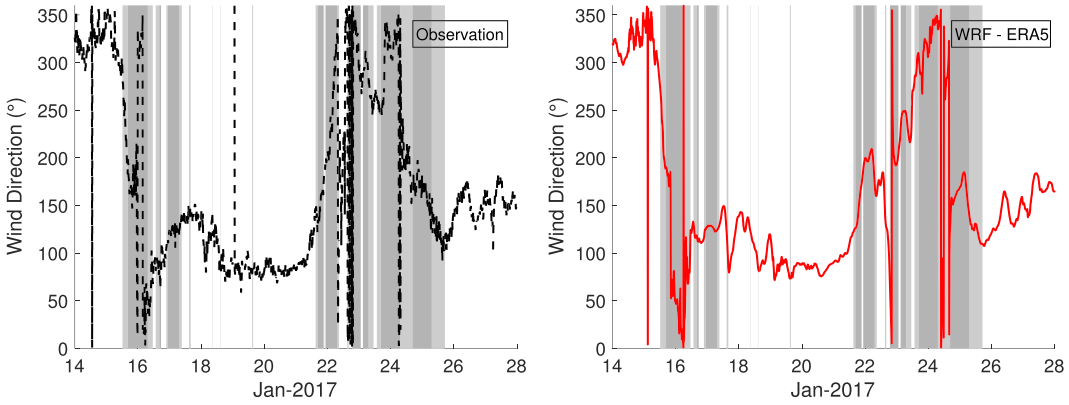


FIGURE 6 Left panel: measured hub height (100 m) wind direction time series at the BWFZ station. Right panel: simulated wind direction time series (96 m) extracted from the WRF–ERA5 run (d02 domain). The selected grid point from the WRF model is in close proximity of the BWFZ station. The daytime Dunkelflaute periods are represented with lightly shaded gray regions. The weak wind conditions, occurring during nighttime hours (no solar power generation), are demarcated by a darker shade [Colour figure can be viewed at wileyonlinelibrary.com]

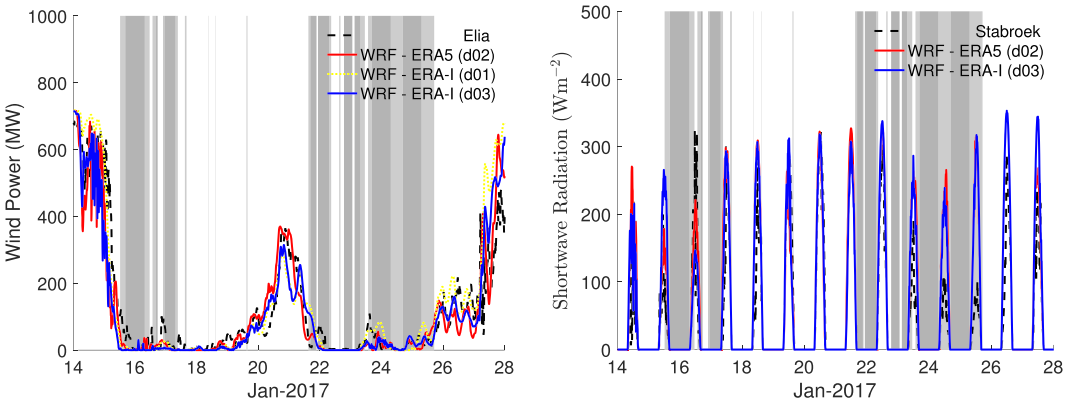


FIGURE 7 Left panel: measured and simulated wind power production data. The measured data are obtained from Elia. Right panel: comparison of measured and simulated (downwelling) shortwave radiation data. The automated weather station is located at Stabroek, Belgium. Only the simulated data from the innermost domains (i.e., grid size of 3 km) of the WRF–ERA5 and WRF–ERA-I runs are shown in these plots. The daytime Dunkelflaute periods are represented with lightly shaded gray regions. The weak wind conditions, occurring during nighttime hours (no solar power generation), are demarcated by a darker shade [Colour figure can be viewed at wileyonlinelibrary.com]

The measured and simulated air temperature time-series are compared in the left panel of Figure 8. Once again, we have selected the BWFZ location for comparison. The temperature data were measured at a height of 4 m. However, the simulated data are from 2-m height. In spite of the height difference, the measured and simulated data portray similar trends. As often happens in marine boundary layers, no sign of a diurnal cycle can be found in the temperature data during January 14th–28th. However, during this period, the air temperature dipped below freezing twice, due to the passages of cold fronts. Such temperature drops increased the energy demand, and in turn, the energy deficits during the Dunkelflaute event.

The simulated sea-surface temperature (SST) and surface sensible heat flux values from BWFZ are shown in the left and right panels of Figure 8, respectively. During the two-week simulation period, the SST decreased marginally. Because SST was almost always higher than the air temperature, there is expected to be positive sensible heat flux at the surface. Under such meteorological conditions, the surface layer is considered to be unstable (convective) and it promotes turbulent mixing. Wind shears decrease drastically due to mixing as depicted earlier in Figure 5.

During January 27th–28th, due to warm air advection, the air temperature became warmer than the sea-surface and created stably stratified conditions. Such atmospheric conditions are conducive to high wind shears as can be seen in Figure 5.

6.2 | Boundary layer structure

Measured profiles of potential temperature and wind speed spanning the entire boundary layer are not available over the southern part of the North Sea region. As a substitute, we utilize radiosondes launched from three neighboring locations over land (Herstmonceux, Norderney, and EDZE Essen; see right panel of Figure 4) to characterize the boundary layer structure. In Figures 9–11, we compare measured and simulated profiles for January 15th and 24th. For both days, we show profiles corresponding to 00 UTC (close to local midnight) and 12 UTC (close to local noon time). Simulated data from three runs (WRF–ERA5, WRF–ERA5#, and WRF–ERA-I) are considered. In addition, we also plot the vertical profiles which are directly extracted from the ERA5 reanalysis data.

Overall, all the simulations and ERA5 data more-or-less capture the magnitudes and shapes of the profiles. Among them, the ERA5 is a clear winner and the WRF–ERA-I performs the worst. The performances of the WRF–ERA5 and WRF-ERA5# runs are slightly poorer than ERA5. This reduction in performance is possible because the WRF runs only utilize ERA5 data during initialization and as boundary conditions. All the internal grid points of the WRF domains dynamically evolve without any data assimilation. The effects of grid nudging is felt only above 2 km.

Because the radiosondes were launched over land, the potential temperature profiles often portray the telltale signs of the circadian cycles. For example, nocturnal stably stratified conditions are noticeable at Herstmonceux (00 UTC of January 15th and 24th), Norderney (00 UTC of January 24th), and EDZE Essen (00 UTC of January 15th and 24th). The daytime unstable conditions (mixed profiles) are evident at Herstmonceux (12 UTC of January 24th), Norderney (12 UTC of January 15th and 24th), and EDZE Essen (12 UTC of January 24th). The other potential temperature profiles do not follow a canonical diurnal pattern. For example, at 12 UTC of January 15th, a deep stable layer persists over Herstmonceux and EDZE Essen.

The WRF simulations have, most of the time, captured the shape and amplitudes of the potential temperature profiles. However, they failed to capture the mixed layer evolution on January 24th at Herstmonceux and EDZE Essen. They underestimated the residual layer height at

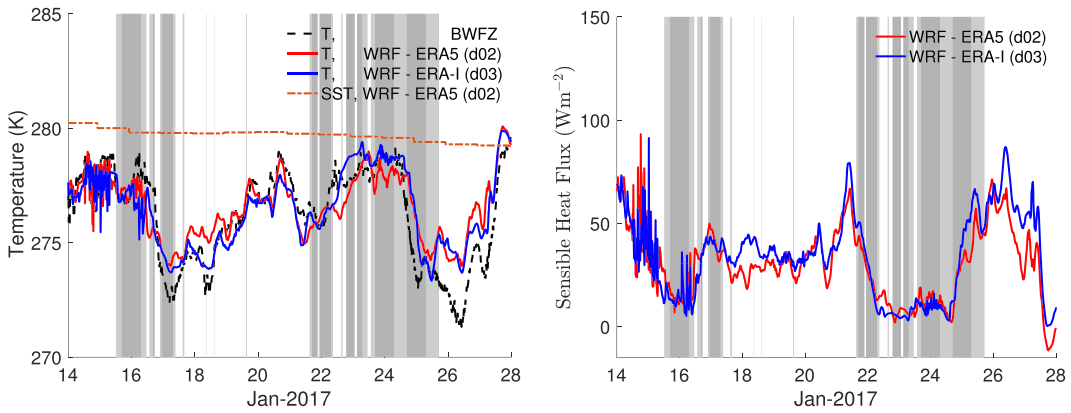


FIGURE 8 Left panel: measured and simulated air temperature time series at the BWFZ station. The measurement height was 4 m; whereas, the simulated data are from 2 m height. The simulated sea-surface temperature (SST) is also overlaid for comparison. Right panel: temporal evolution of sensible heat flux at the surface from the WRF simulations. Only the simulated data from the innermost domains (i.e., grid-size of 3 km) of the WRF–ERA5 and WRF–ERA-I runs are shown in these plots. The daytime Dunkelflaute periods are represented with lightly shaded gray regions. The weak wind conditions, occurring during nighttime hours (no solar power generation), are demarcated by a darker shade [Colour figure can be viewed at wileyonlinelibrary.com]

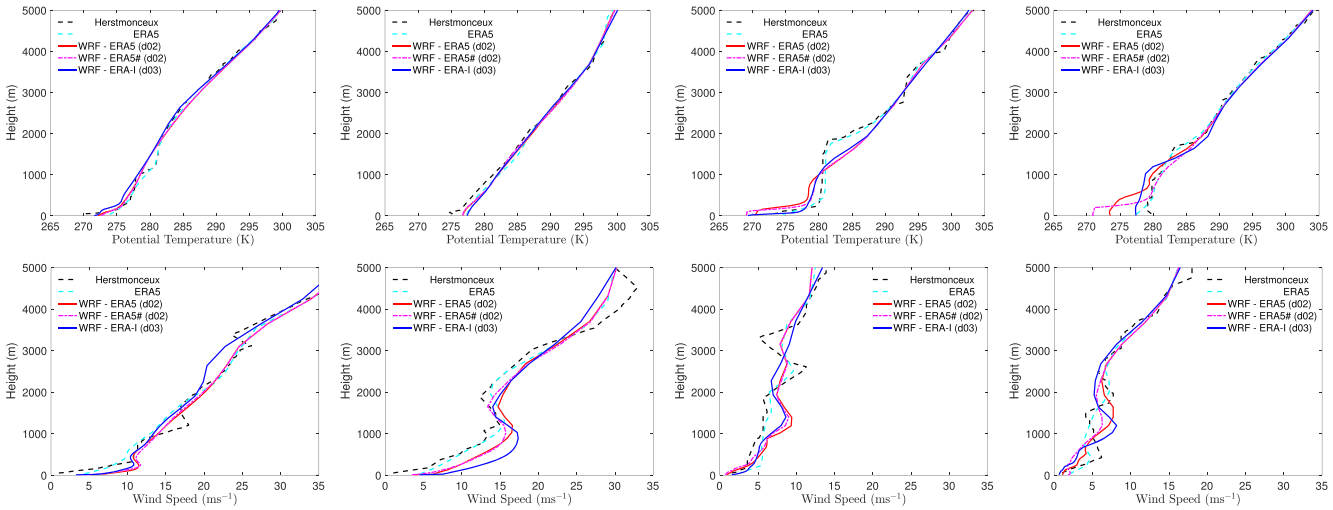


FIGURE 9 Observed and simulated potential temperature (top panel) and wind speed (bottom panel) profiles at the Herstmonceux radiosonde launch location. From left to right, the plots correspond to the following times, respectively: 00 UTC of January 15th, 12 UTC of January 15th, 00 UTC of January 24th, and 12 UTC of January 24th. For the WRF runs (i.e., WRF–ERA5, WRF–ERA5#, and WRA–ERA-I), only the simulated results from the 3 km domains are shown and compared. Extracted data from the ERA5 reanalysis data are also included as a baseline [Colour figure can be viewed at wileyonlinelibrary.com]

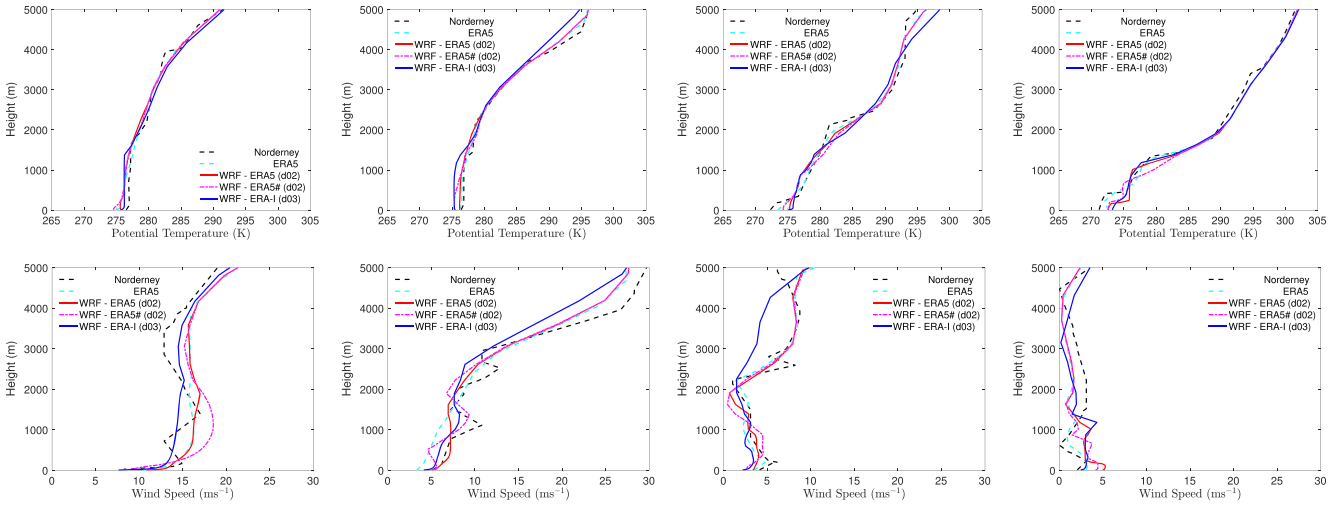


FIGURE 10 Same as Figure 9, except for the Norderney radiosonde launch station [Colour figure can be viewed at wileyonlinelibrary.com]

00 UTC. The growth of the mixed layer is rather slow for all the simulations. In comparison to the MYNN scheme, the YSU scheme significantly delays the formation of the mixed layer. It is plausible that the entrainment rate is better simulated by the MYNN scheme for this specific case.

The observed wind speeds at higher altitudes were quite strong on January 15th and the simulated ones closely resembled them. However, the WRF results overestimated the turbine-layer wind speeds at Herstmonceux. On January 24th, the wind speeds subsided drastically. At all the locations, the observed and simulated wind speeds were approximately 5 m s^{-1} or even weaker in the lowest 1 km of the boundary layer.

In lieu of observed boundary layer profiles near the Belgian offshore wind farm region, we only document simulated time-height plots of wind speeds and potential temperatures in Figure 12. The estimated PBL heights are overlaid on these plots. From the temperature plot, it is clear that the PBL height was rather shallow (less than 500 m) for the large part of the 2-week simulation period. Furthermore, the temperature profiles are found to be uniform in height (i.e., well-mixed) within the boundary layer for most of the time. This result further corroborates our previous finding that the marine boundary layer near the BWFZ station was unstable during January 14th–27th of 2017.

The top-left panel of Figure 12 suggests that a sudden reduction of the wind speed happens on January 15th and persists until January 21st. The gentle breezy condition returned again on January 22nd and lasted until January 27th. The depth of the weak flow field extends much higher

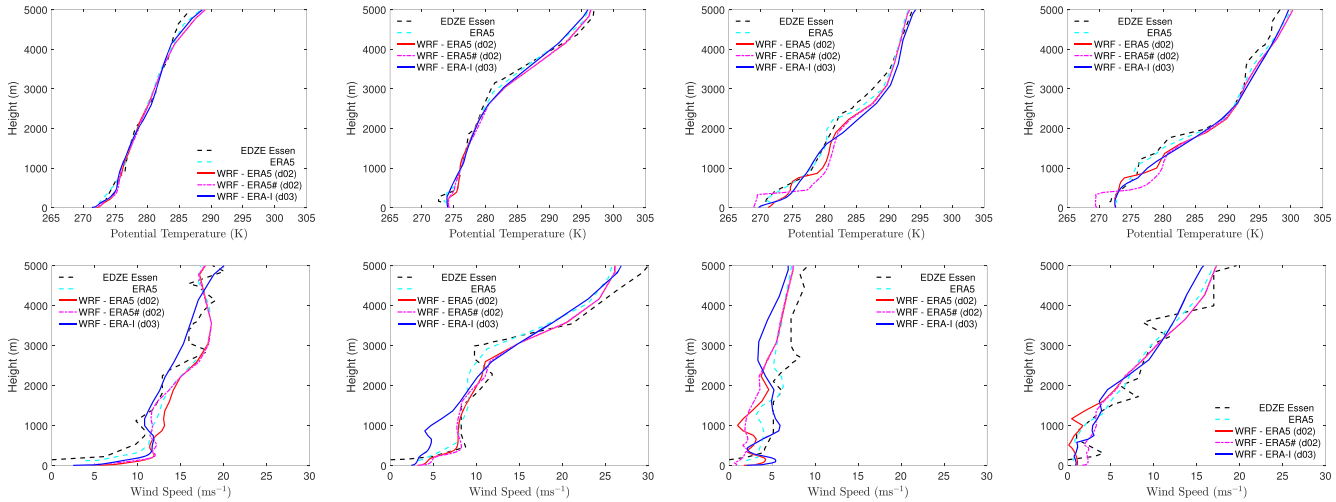


FIGURE 11 Same as Figure 9, except for the EDZE Essen radiosonde launch station [Colour figure can be viewed at wileyonlinelibrary.com]

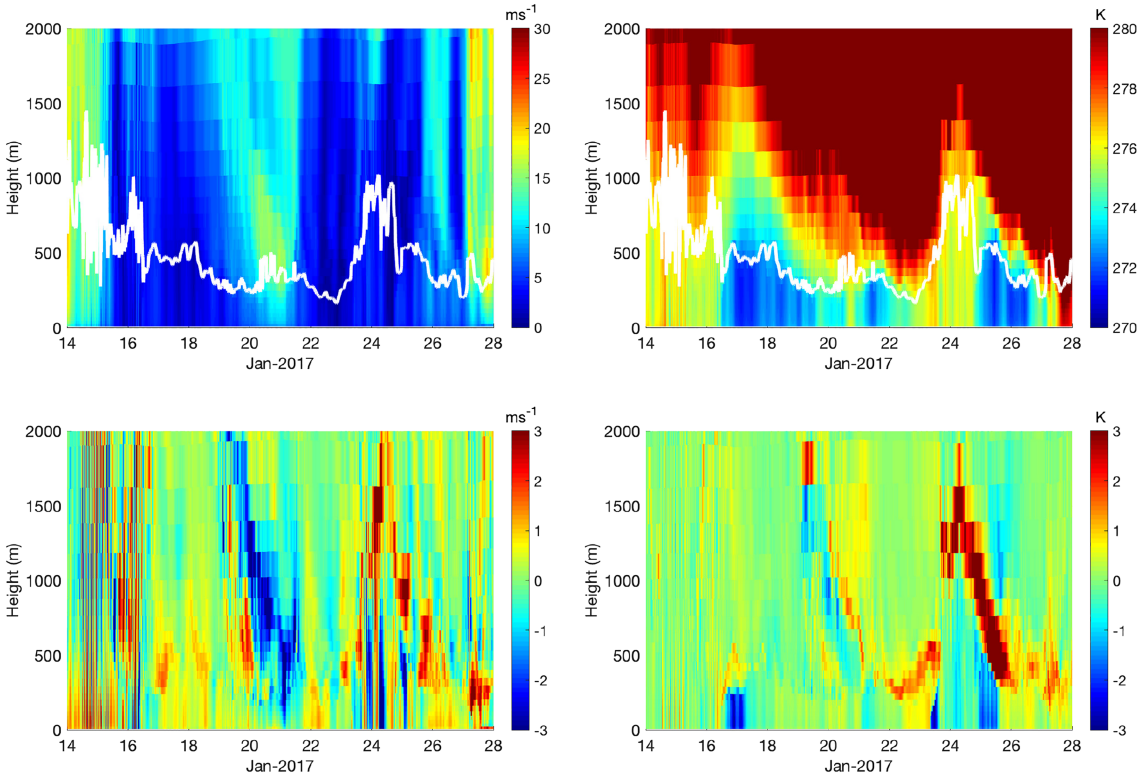


FIGURE 12 Time-height plots of simulated wind speeds (top-left panel) and potential temperature (top-right panel) from the d02 domain (grid size of 3 km) of the WRF–ERA5 run. The simulated PBL heights are overlaid on these plots as white lines. Time-height plots of the differences between the WRF–ERA5# and WRF–ERA5 runs (d02 domains) are shown in the bottom panels. The bottom-left and bottom-right panels represent differences of wind speeds and potential temperatures, respectively. The grid point closest to the BWFZ station is selected for all these plots [Colour figure can be viewed at wileyonlinelibrary.com]

than the PBL height. Thus, it is caused by a synoptic scale system (an anticyclone) and not modulated by boundary layer processes. The localized increase of wind speeds on January 21st could be due to an offshore low-level jet; it is a mere speculation and cannot be substantiated in this study.

In order to quantify the impact of the PBL schemes on the simulated results, we have computed the differences of simulated results from the WRF–ERA5# run (invokes the YSU PBL scheme) and the WRF–ERA5 run (utilizes the MYNN 2.5 level PBL scheme). The time-height plots of the

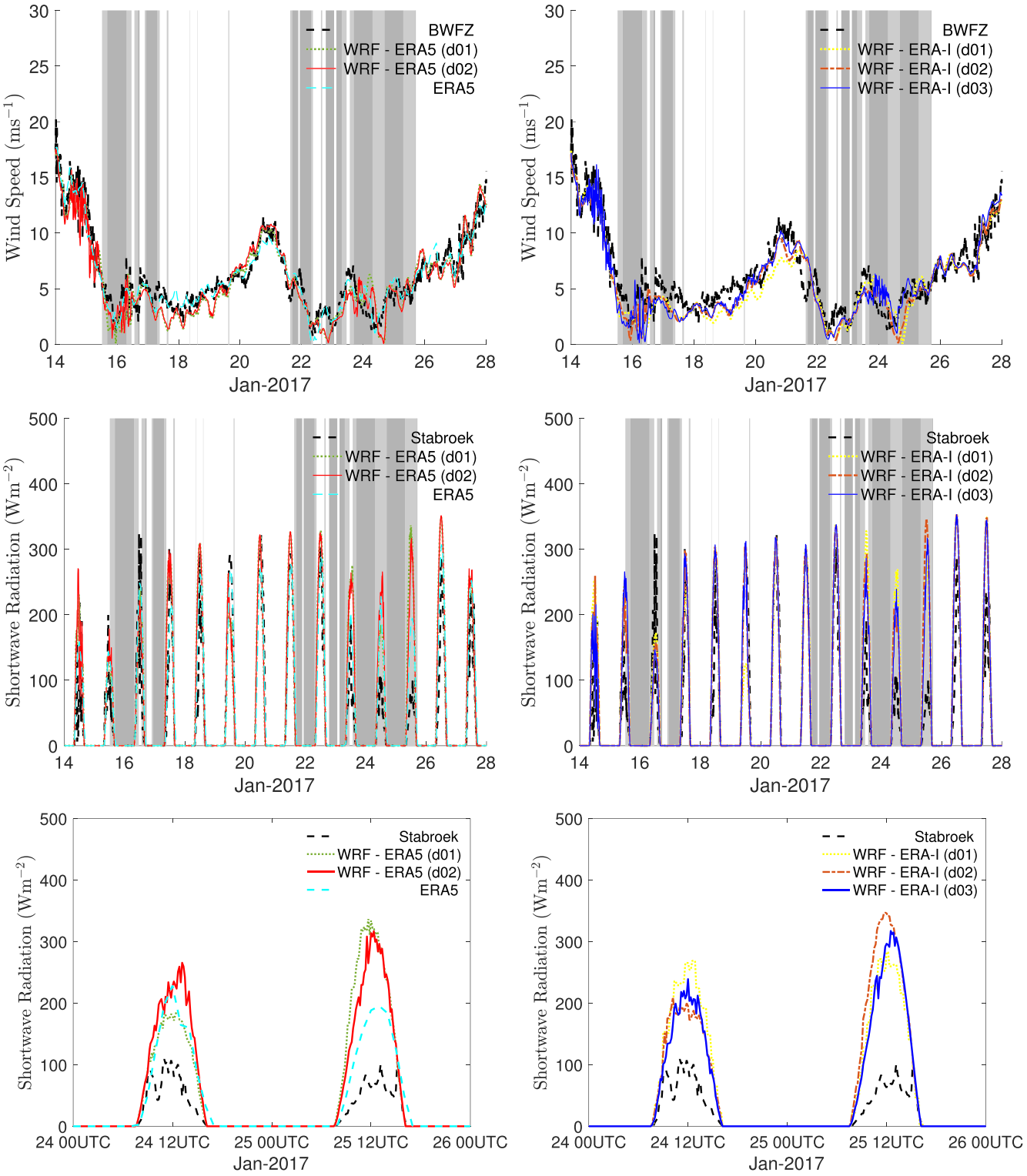


FIGURE 13 Measured and simulated wind speed time series (top panels) and (downwelling) shortwave radiation (middle panels) for January 14th–28th. The bottom panels show measured and simulated shortwave radiation time series for a shorter duration of January 24th–25th for clarity. The observational wind speeds and radiation data are from the BWFZ station and Stabroek station, respectively. Simulated results from all the computational domains of the WRF–ERA5 (left panels) and WRF–ERA-I (right panels) are plotted for comparison. Extracted data from the ERA5 reanalysis data are also included as a baseline. The daytime Dunkelflaute periods are represented with lightly shaded gray regions. The weak wind conditions, occurring during nighttime hours (no solar power generation), are demarcated by a darker shade [Colour figure can be viewed at wileyonlinelibrary.com]

differences of wind speeds and potential temperatures are shown in the bottom panel of Figure 12. In terms of potential temperature, the differences are not large. Most of the differences occur in the (subsidence) inversion zone overlying the boundary layer. The wind speed values also differ significantly within this zone. Within the PBL, the YSU scheme often produces slightly stronger wind speeds in comparison to the MYNN scheme.

6.3 | Sensitivity to grid-size and IC/BC

The observed and simulated hub-height (~100 m) wind speeds from the BWFZ location are shown in the top panel of Figure 13. The simulated time series from WRF-ERA5 and WRF-ERA-I are quite similar. More interestingly, for both the runs, the simulated results are virtually insensitive to grid-sizes. The ERA5 reanalysis data match the observed data remarkably well, as found earlier in the context of vertical profiles.

In the context of (downwelling) shortwave radiation, the differences between different simulations are significant (see the middle and bottom panel of Figure 13). All the WRF-based results overestimate the magnitude of radiation during the Dunkelflaute periods. For other times, the simulated results are not too far off from from the observations.

6.4 | Sensitivity to wind farm parameterization

The numerical configuration and the physical parameterization options of the WRF–ERA5* run are identical to the default run WRF–ERA5. Except, in the WRF–ERA5* run, the wind farm parameterization scheme is turned off. Whereas, in the WRF–ERA5 run, it is used in conjunction with 182 wind turbines. The differences in the simulated wind speeds and turbulent kinetic energy at the BWFZ station are shown in Figure 14.

The BWFZ station is located about 10 km from the Belgian offshore wind farms (refer to the left panel of Figure 4). It can experience wind farm wake effects when the prevailing wind direction is within 180–270 degrees. According to Figure 6, such wind directions happened a few times during Jan 14th–28th. During such periods (e.g., January 16th and 24th), the wake effects can be clearly seen in Figure 14. These differences are quite substantial in terms of both mean wind speeds and turbulent kinetic energy. For other periods, there are small differences as well. This is due to the fact that in mesoscale simulations any perturbations (here imposed by the wind farm parameterization) in flow fields change future evolution (the so-called "butterfly effect").

6.5 | Reanalysis versus real-time

In addition to initial fields, the WRF model (or any other mesoscale model) requires boundary conditions spanning the entire simulation period. For retrospective simulations, such boundary conditions can be extracted from the reanalysis datasets (e.g., ERA5 and ERA-Interim). Due to extensive data assimilation, such boundary conditions tend to be very accurate. However, in the context of real-time forecasting, such high-fidelity boundary conditions are not available. Rather, one has to use operational forecast data from a global model (e.g., GFS).

In this section, we compare the results from the WRF−GFS run against the default WRF−ERA5 run. We expect the accuracy of the WRF−GFS to be comparable with WRF−ERA5 run at the beginning of the simulation period; however, its performance will likely deteriorate with

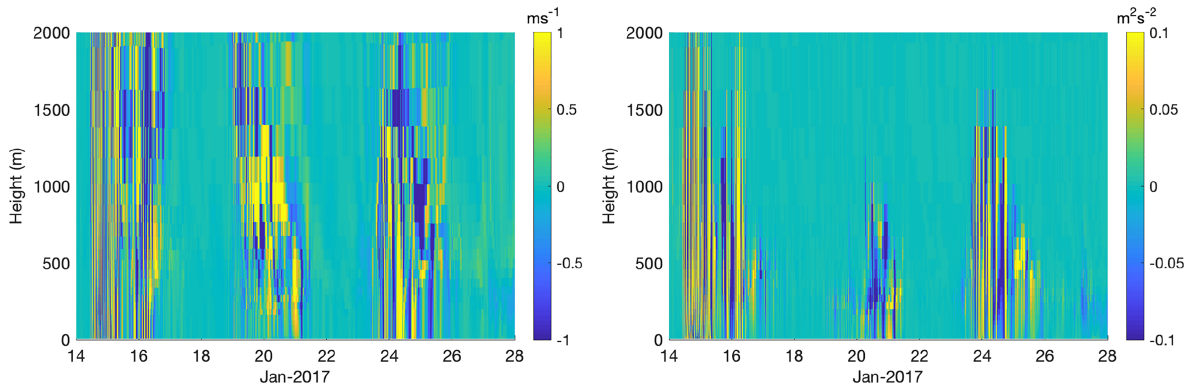


FIGURE 14 Time-height plots of the differences between the WRF–ERA5 and WRF–ERA5* runs (d02 domains). The left and right panels represent differences of wind speeds and turbulent kinetic energy, respectively. The grid point closest to the BWFZ station is selected for all these plots [Colour figure can be viewed at wileyonlinelibrary.com]

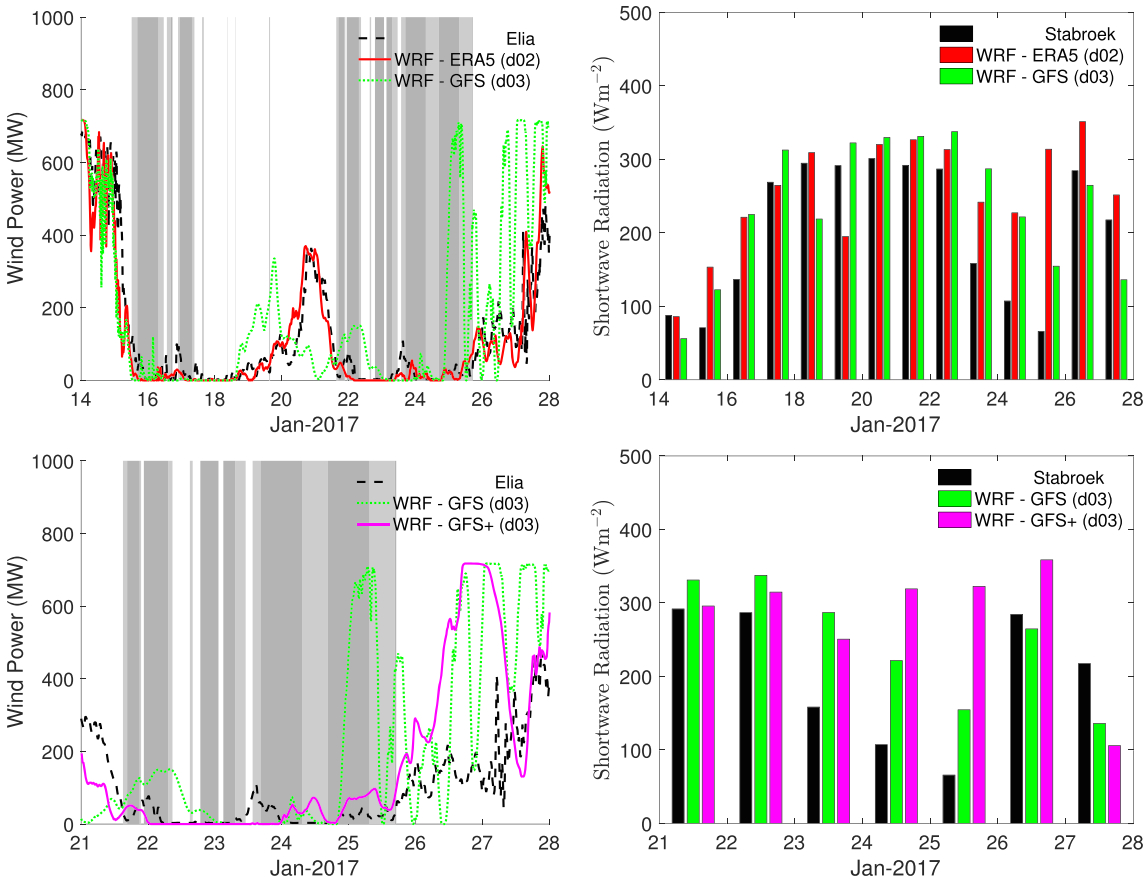


FIGURE 15 Measured and simulated wind power production data (top-left panel) and (downwelling) solar radiation at 12 UTC during January 14th–28th (top-right panel). The simulated results from WRF–GFS+ run, initialized on January 21st, are shown in the bottom panel. The measured wind power data are obtained from Elia. Only the simulated data from the innermost domains (i.e., grid-size of 3 km) of the WRF–ERA5 and WRF–GFS runs are shown in these plots. The daytime Dunkelflaute periods are represented with lightly shaded gray regions. The weak wind conditions, occurring during nighttime hours (no solar power generation), are demarcated by a darker shade [Colour figure can be viewed at wileyonlinelibrary.com]

increasing prediction horizon. The top-left panel of Figure 15 is in line with our expectation. During the period of January 14th–18th, in terms of wind power production, the performance of the WRF–GFS run is at par with WRF–ERA5. Afterwards, its results deviate significantly from the measured data from Elia. Even though the WRF–GFS run predicts the commencement of the second Dunkelflaute period rather accurately, it underestimates its duration. It predicts that the power output from the Belgian wind farms return to the nameplate capacity level by January 25th; in reality, such recovery happened after January 28th. In contrast, the WRF–GFS+ run, initialized on January 21st, significantly improves the quality of the wind power forecast for the second Dunkelflaute period (particularly during January 21st–26th) due to the reduction in prediction horizon (refer to bottom-left panel of Figure 15). In terms of (downwelling) shortwave radiation, the performance of the WRF–ERA5, WRF–GFS, and WRF–GFS+ runs are poor (right panel of Figure 15). More validation work, potentially involving satellite remote-sensing-based radiation data, is needed in this arena.

7 | CONCLUDING REMARKS

In this work, we simulate and characterize a Dunkelflaute (aka anticyclonic gloom) event via mesoscale modeling. An extensive suite of observational data assisted in the model validation. In addition to weak wind and cloudy conditions, we have found that the marine boundary layer was frequently well-mixed during this event. As a consequence, wind speed shears were negligible in measurements over the North Sea and also in corresponding simulated data. Over land, however, the observed and simulated profiles portray traits of stratification and wind speed shears.

For basic climatological characterizations of Dunkelflaute events, the ERA5 reanalysis dataset could be utilized owing to its global coverage, long-term availability, and high accuracy. However, this dataset does not include the wake effects of wind farms. In order to account for such

effects, one should utilize the WRF model or other mesoscale models in conjunction with a suitable wind farm parameterization. Mesoscale simulations can also provide more advanced diagnostics (e.g., turbulent kinetic energy), and by virtue of their high spatial resolutions, they can resolve coastal effects.

In this study, we have noticed that in retrospective mode, some of the features (e.g., hub height wind speeds and power production) of the Dunkelflaute can be reliably simulated using coarse grid-sizes (e.g., 27 km). If this finding holds true for modeling of other Dunkelflaute events, then it will be possible to simulate these events with relatively low computational costs. In a real-time forecasting scenario, however, this specific event could not be predicted beyond four days. In our future work, we will find out if we can improve on the predictability of these events by coupling mesoscale modeling with deep learning approaches.

Before closing, we would like to mention that the renewable energy community is not the only stakeholder who is interested in a better understanding and forecasting capability of the Dunkelflaute phenomenon. It is also relevant for the air pollution community[53,54] and the astronomy community.[55]

ACKNOWLEDGEMENTS

Sukanta Basu thanks Jacob van Berkel for introducing him to the Dunkelflaute phenomenon. We are grateful to Elia for making the Belgian offshore wind power production data publicly available. We also thank Royal Meteorological Institute of Belgium for sharing their automated weather station data. We greatly appreciate the assistance of Pim van Dorp for identifying the locations of the wind turbines in the Belgian wind farms. This study benefited by having useful discussions with Stephan de Roode.

CONFLICT OF INTEREST

The authors declare no potential conflict of interests.

PEER REVIEW

The peer review history for this article is available at https://publons.com/publon/10.1002/we.2554.

ORCID

Sukanta Basu https://orcid.org/0000-0002-0507-5349
Simon J. Watson https://orcid.org/0000-0001-6694-3149

REFERENCES

1. European Commission. Report from the Commission to the European Parliament, the Council, the European Economic and Social Committee and the committee of the regions on the implementation of EU macro-regional strategies. Technical Report, European Commission, Brussels, Belgium; 2019. https://eur-lex.europa.eu/legal-content/EN/TXT/?uri=COM:2019:21:FIN. Accessed June 19, 2019.
2. European Commission. *Energy Roadmap 2050*. Belgium: Publications Office of the European Union; 2012.
3. Müller M, Haesen E, Ramaekers L, Verkaik N. Translate COP21—2045 outlook and implications for offshore wind in the North Seas. Technical Report, Ecofys; 2017. Online: https://www.ecofys.com/en/publications/translate-cop21/. Accessed June 20, 2019.
4. CONCERE. National Energy and Climate Plans (NECPs)—Brussels, Belgium. Plan National intégré energie climat belge 2021-2030. Technical Report, Commission nationale Climat; 2018. https://ec.europa.eu/energy/sites/ener/files/documents/belgium_draftnecp_fr.pdf. Accessed June 20, 2019.
5. Energy Agenda: Towards a low-carbon energy supply. Technical Report, The Netherlands, Ministry of Economic Affairs; 2017. https://www.government.nl/binaries/government/documents/reports/2017/03/01/energy-agenda-towards-a-low-carbon-energy-supply/Energy+agenda.pdf. Accessed June 20, 2019.
6. Huneke F, Perez Linkenheil C, Niggemeier M. Kalte Dunkelflaute: Robustheit des Stromsystems bei Extremwetter. Technical Report, Berlin, Energy Brain Pool, Greenpeace Energy; 2017.
7. NOS. Netbeheerder moest groot inkopen om stroomtekort op te vangen. https://nos.nl/artikel/2229787-netbeheerder-moest-groot-inkopen-om-stroomtekort-op-te-vangen.html. Accessed June 20, 2019; 2018.
8. NRC. Netbeheerder Tennet wendt landelijk stroomtekort af. https://www.nrc.nl/nieuws/2018/04/30/landelijk-stroomtekort-afgewend-door-netbeheerder-tennet-a1601355. Accessed June 20, 2019; 2018.
9. VRT. België telde negen dagen Dunkelflaute in januari. https://www.vrt.be/vrtnws/nl/2017/02/24/belgie_telde_negendagendunkelflauteinjanuari-1-2900900/. Accessed June 20, 2019; 2017.
10. Elia. Electricity Scenarios for Belgium towards 2050, Elia's Quantified Study on the Energy Transition in 2030 and 2040. Technical Report, Elia, Brussels, Belgium; 2017.
11. Meinke-Hubeny F, de Oliveira LPN, Duerinck J, Lodewijks P, Belmans R. Energy Transition in Belgium–Choices and Costs. Technical Report, EnergyVille in opdracht van Febeliec, Genk, Belgium; 2017.
12. CREG. Study on the functioning and price evolution of the Belgian wholesale electricity market—monitoring report 2017. Technical Report F1734, Commission for Electricity and Gas Regulation, Brussels, Belgium; 2018.
13. Wetzel D. Die Dunkelflaute bringt Deutschlands Stromversorgung ans Limit. https://www.welt.de/wirtschaft/article161831272/Die-Dunkelflaute-bringt-Deutschlands-Stromversorgung-ans-Limit.html. Accessed June 20, 2019; 2017.

14. Schultz S. Ist der Winter wirklich zu düster für den Ökostrom? https://www.spiegel.de/wirtschaft/soziales/oekostrom-knapp-panikmache-mit-der-dunkelflaute-a-1133450.html. Accessed June 20, 2019; 2017.
15. Wissenschaftliche Dienste. Sicherstellung der Stromversorgung bei Dunkelflauten. Technical Report WD 5 - 3000 - 167/18, Deutscher Bundestag, WD 5: Wirtschaft und Verkehr, Ernährung, Landwirtschaft und Verbraucherschutz, Berlin, Germany; 2019.
16. Skamarock WC, Klemp JB. A time-split nonhydrostatic atmospheric model for weather research and forecasting applications. *J Comput Phys*. 2008; 227(7):3465-3485.
17. Skamarock WC, Klemp JB, Dudhia J, et al. A description of the advanced research WRF version 3. NCAR technical note-475+; STR, Boulder, Colorado, USA; 2008. http://dx.doi.org/10.5065/D68S4MVH
18. Watts A. *Weather wise: Reading weather signs*. Adlard Coles, Bloomsbury Publishing; 2013. https://www.bloomsbury.com/uk/weather-wise-9781408127087/
19. Perkins O. *Reading the clouds: How you can forecast the weather*. Adlard Coles, Bloomsbury Publishing; 2018. https://www.bloomsbury.com/uk/reading-the-clouds-9781472960177/
20. Robinson DN. Describing the weather in Lincolnshire dialect. *Weather*. 1968;23:72-74.
21. Douglas CKM. Clouds as seen from an aeroplane. *Q J Roy Meteor Soc*. 1920;46(195):233-242.
22. Allaby M. *Encyclopedia of weather and climate*. Facts on File; 2007. https://books.google.nl/books?id=J1wq-9OSCscC
23. Weller J, Thornes JE. An investigation of winter nocturnal air and road surface temperature variation in the West Midlands, UK under different synoptic conditions. *Meteorol Appl*. 2001;8(4):461-474.
24. Galvin J. Anticyclonic gloom. *Weather*. 2004;59:236-236.
25. Priestley CHB, Swinbank WC. Vertical transport of heat by turbulence in the atmosphere. *Proc Roy Soc Lon Ser A*. 1947;189:543-561.
26. Robinson GD. The vertical convective heat flux in the atmosphere–a critical essay. *Q J Roy Meteor Soc*. 1951;77(331):61-73.
27. Moeng C-H. Large-eddy simulation of a stratus-topped boundary layer. Part I: Structure and budgets. *J Atmos Sci*. 1986;43:2886-2900.
28. Duynkerke PG, de Roode SR, van Zanten MC, et al. Observations and numerical simulations of the diurnal cycle of the EUROCS stratocumulus case. *Q J Roy Meteorol Soc*. 2004;130:3269-3296.
29. Stevens B, Moeng C-H, Ackerman AS, et al. Evaluation of large-eddy simulations via observations of nocturnal marine stratocumulus. *Mon Wea Rev*. 2005;133:1443-1462.
30. ENTSOG. Winter Review 2016/2017. Technical Report SO0017-17, European Network of Transmission System Operators for Gas, Brussels, Belgium; 2017.
31. Anagnostopoulou C, Tolika K, Lazoglou G, Maheras P. The exceptionally cold January of 2017 over the Balkan Peninsula: A climatological and synoptic analysis. *Atmosphere*. 2017;8(12):252.
32. DNV-GL. Assessment wind measurement program North Sea. 14-2781, Rev. 1: ; 2014. 57 pp; 2014.
33. Clement-Nyns K. Forecast and actual wind power generation. Technical Report, Elia, Brussels, Belgium; 2016. https://www.elia.be/\textasciitilde/media/files/Elia/Grid-data/Power%20Generation/WindForecasting_EN.pdf. Accessed July 17, 2020.
34. Smet J. Forecast and actual solar-PV power generation. Technical Report, Elia, Brussels, Belgium; 2017. https://www.elia.be/\textasciitilde/media/files/Elia/Grid-data/Power%20Generation/SolarForecasting_EN.pdf. Accessed July 17, 2020.
35. Fugro Norway AS. Supply of Meteorological and Oceanographic data at Borssele Wind Farm Zone (BWFZ), Monthly Progress Report: Period 26 December 2016- 26 January 2017. Technical Report C75339_MPR15_R1 prepared for the Netherlands Enterprise Agency (RVO), Utrecht, Netherlands; 2017. https://offshorewind.rvo.nl/file/download/49027622/Data+;%26amp%3B+;Validation+;report+;Period+;15+;-+;Fugro. Accessed July 17, 2020.
36. Fugro Norway AS. Supply of Meteorological and Oceanographic data at Borssele Wind Farm Zone (BWFZ), Monthly Progress Report Period: 26 January- 26 February 2017. Technical Report C75339_MPR16_R1 prepared for the Netherlands Enterprise Agency (RVO), Utrecht, Netherlands; 2017. https://offshorewind.rvo.nl/file/download/50256672/Data+;%26amp%3B+;Validation+;report+;Period+;16+;-+;Fugro. Accessed July 17,2020.
37. Fugro Norway AS. Supply of Meteorological and Oceanographic data at Hollandse Kust (zuid), Monthly Progress Report Period: January 2017. Technical Report prepared for the Netherlands Enterprise Agency (RVO), Utrecht, Netherlands; 2017. https://offshorewind.rvo.nl/windwaterzh. Accessed July 17, 2020.
38. Fugro Norway AS. Hollandse Kust (zuid) Field Measurement Campaign, Validation Report - January 2017. Technical Report prepared for the Netherlands Enterprise Agency (RVO), Utrecht, Netherlands; 2017. https://offshorewind.rvo.nl/windwaterzh. Accessed July 17, 2020.
39. ECN. LEG: Introductie. https://windopzee.net/lichteiland-goeree-leg/. Accessed July 4, 2019; 2016.
40. ECN. EPL: Introductie. https://windopzee.net/europlatform-epl/. Accessed July 4, 2019; 2016.
41. RMI. Automatic weather station (AWS) daily observations. https://data.gov.be/en/dataset/aws1day. Accessed July 4, 2019; 2016.
42. Wyoming University. Wyoming atmospheric soundings. http://weather.uwyo.edu/upperair/sounding.html. Accessed November 13, 2019; 2019.
43. Chen F, Dudhia J. Coupling an advanced land surface–hydrology model with the Penn State–NCAR MM5 modeling system. *Mon Weather Rev*. 2001; 129(4):587-604.
44. Iacono MJ, Delamere JS, Mlawer EJ, Shephard MW, Clough SA, Collins WD. Radiative forcing by long-lived greenhouse gases: calculations with the AER radiative transfer models. *J Geophys Res Atmos*. 2008;113:D13103.
45. Hong SY, Dudhia J, Chen SH. A revised approach to ice microphysical processes for the bulk parameterization of clouds and precipitation. *Mon Weather Rev*. 2004;132(1):103-120.
46. Kain JS. The Kain–Fritsch convective parameterization: an update. *J Appl Meteorol*. 2004;43(1):170-181.
47. Nakanishi M, Niino H. An improved Mellor–Yamada level-3 model: its numerical stability and application to a regional prediction of advection fog. *Bound-Lay Meteorol*. 2006;119(2):397-407.
48. Hong SY, Noh Y, Dudhia J. A new vertical diffusion package with an explicit treatment of entrainment processes. *Mon Weather Rev*. 2006;134(9): 2318-2341.
49. Hong S-Y. A new stable boundary-layer mixing scheme and its impact on the simulated East Asian summer monsoon. *Q J Roy Meteorol Soc*. 2010;136: 1481-1496.
50. Fitch AC, Olson JB, Lundquist JK, et al. Local and mesoscale impacts of wind farms as parameterized in a mesoscale NWP model. *Mon Weather Rev*. 2012;140(9):3017-3038.

51. C3S. Era5: Fifth generation of ecmwf atmospheric reanalyses of the global climate. https://cds.climate.copernicus.eu/cdsapp\#!/home. Accessed February 20, 2020; 2017.
52. Berrisford P, Dee DPKF, Fielding K, et al. The ERA-interim archive. *ERA Rep Ser*. 2009;1:1-16. https://www.ecmwf.int/node/8173
53. Spellman G. Analysing air pollution meteorology. *Weather*. 1998;53:34-42.
54. McGregor GR, Walters S, Wordley J. Daily hospital respiratory admissions and winter air mass types, Birmingham, UK. *Int J Biometeorol*. 1999;43(1):21-30.
55. Varela AM, Bertolin C, Muñoz-Tuñón C, Ortolani S, Fuensalida JJ. Astronomical site selection: on the use of satellite data for aerosol content monitoring. *Mon Not R Astronom Soc*. 2008;391:507-520.
56. Dunstone N, Scaife AA, MacLachlan C, et al. Predictability of European winter 2016/2017. *Atmos Sci Lett*. 2018;19:e868.
57. Bot ETG. Farmflow validation against full scale wind farms. ECN-E–15-045, ECN Wind Energy; 2015. https://publications.ecn.nl/ECN-E--15-045
58. Bulder BH, Bot ETG, Wiggelinkhuizen EJ, Nieuwenhout FDJ. Quick scan wind farm efficiencies of the Borssele location. ECN-E–14-050, ECN Wind Energy; 2015. https://publications.ecn.nl/ECN-E--14-050

How to cite this article: Li B, Basu S, Watson SJ, Russchenberg HWJ. Mesoscale modeling of a "Dunkelflaute" event. *Wind Energy*. 2021;24:5–23. https://doi.org/10.1002/we.2554

APPENDIX A: CLIMATOLOGY OF DUNKELFLAUTE EVENTS IN BELGIUM

We analyzed wind and solar power production data from Elia.be for the years 2013–2018. These data have a sampling rate of 15 min; thus, in a given year, we have approximately 35 000 samples. A particular sample is classified as a Dunkelflaute event if the production by onshore wind, offshore wind, as well as, solar farms fall below 10% of their respective nominal capacities during that particular 15 min period. We do not tag a sample as a Dunkelflaute event if solar power production is exactly zero and it happens outside the time-window of 09 UTC–15 UTC; this way, we effectively exclude nighttime conditions from the climatological analysis. It is clear from Figure A1 that every year all the three renewable power generation sources drop below 10% of their capacities for a substantial period of time (approximately ranging from 30% to 50%). Typically, offshore wind power production has a higher capacity factor in comparison to its onshore counterpart. On average, the Dunkelflaute events account for around 7%–8% of the time per year. These numbers do not vary much across the years.

APPENDIX B: ANOMALY PATTERNS OVER EUROPE

The synoptic condition during the month of January of 2017 was quite unusual as can be seen in Figure B1; see also Dunstone et al.[56] These anomaly plots are created using the ERA5 data. First, a climatological mean is computed for the month of January from ERA5 data spanning the years 1981 to 2010. Then, this mean is subtracted from the monthly average of January 2017.

It is evident that during January 2017, over the North Sea, sea level pressure was a lot higher than the climatological mean over the North Sea region. Similar behavior was observed in the case of 500 mb geopotential height. Both zonal and meridional winds showed negative anomaly for the southern part of North Sea and surrounding areas. Extremely cold conditions prevailed over the southern part of continental Europe.

APPENDIX C: POWER AND THRUST CURVES

The power and thrust curves of the wind turbines from the Belgian offshore wind farms are extracted from various sources (see Table C1) and are plotted in Figure C1. In some cases, in lieu of actual turbine data in the public domain, we had to utilize data from proxy turbines with similar characteristics.

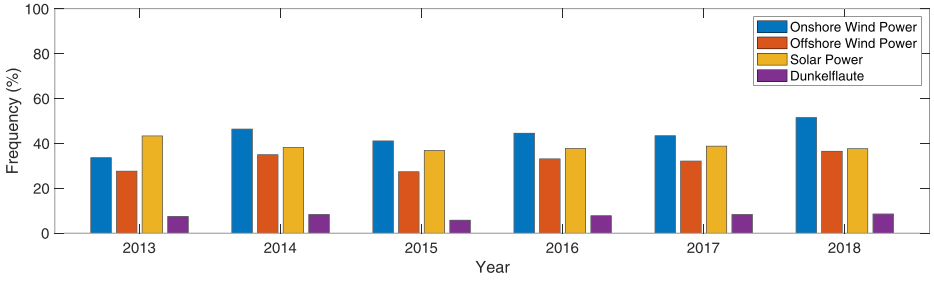


FIGURE A1 Annual climatology of Dunkelflaute events in Belgium. The colored bars represent the percentage of the time when Belgian onshore wind, offshore wind, solar power output, and all three simultaneously (classified as Dunkelflaute) are less than 10% of rated output [Colour figure can be viewed at wileyonlinelibrary.com]

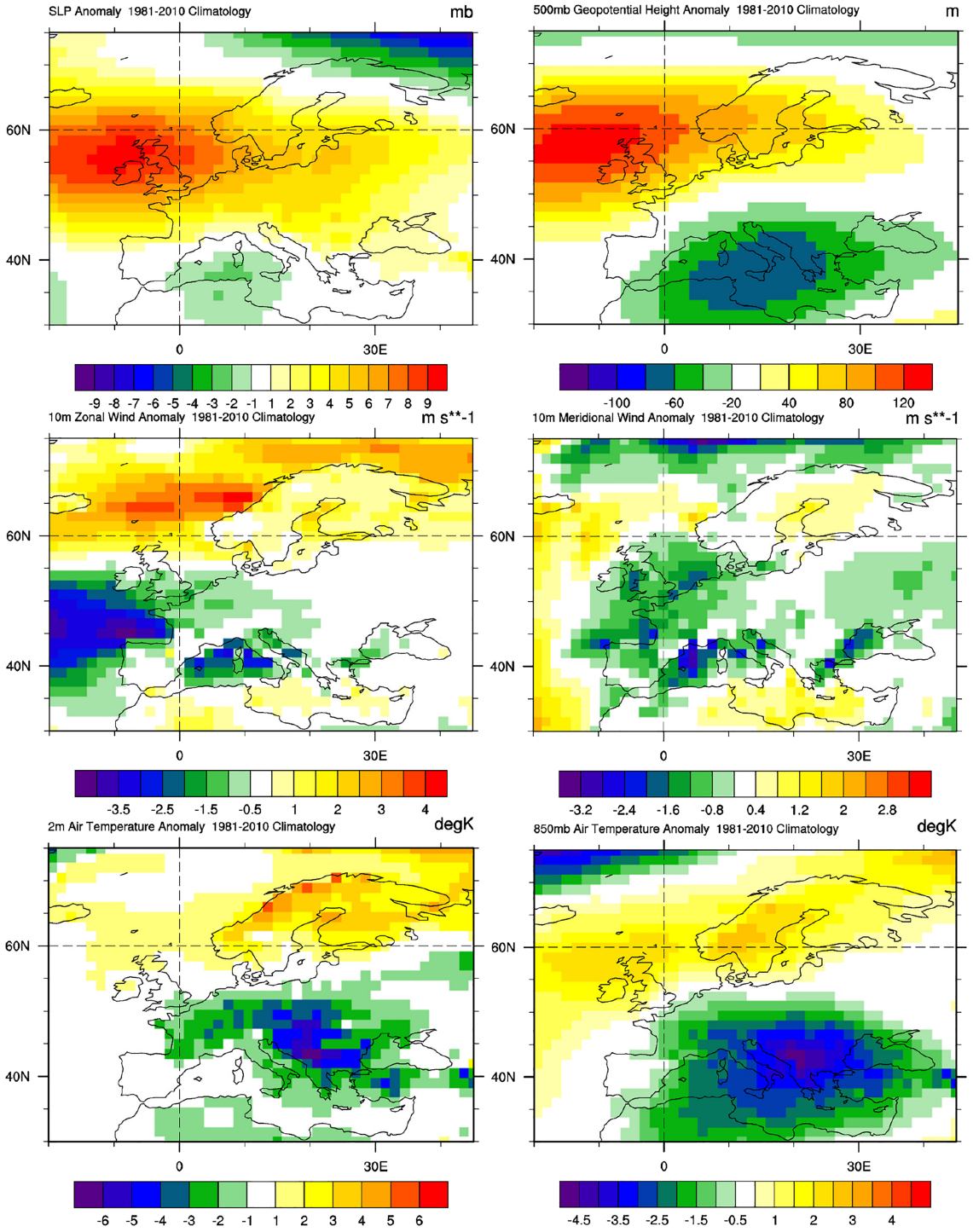


FIGURE B1 Anomaly maps from https://www.esrl.noaa.gov/psd/cgi-bin/data/testdap/plot.comp.pl [Colour figure can be viewed at wileyonlinelibrary.com]

TABLE C1 Sources of power and thrust curves

Turbine	Power Curve	Thrust Curve
Vestas V90 3 MW	Source: manufacturer	Source: Bot, [57]
Vestas V112 3 MW	Source: manufacturer	Source: manufacturer
Senvion (formerly REPower) 5 MW	Source: windPRO	Source: windPRO
Senvion 6.2 MW	Source: manufacturer	Proxy: Senvion 5 MW
Alstom 6 MW	Proxy: ECN 6 MW[58]	Proxy: ECN 6 MW[58]

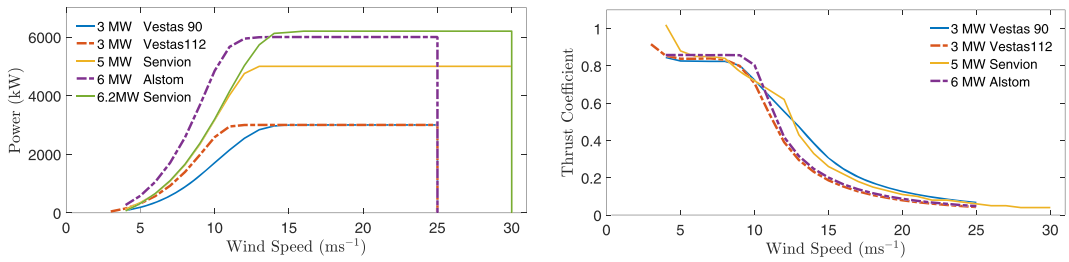


FIGURE C1 Power curves (left panel) and thrust curves (right panel) of the turbines from the Belgian offshore wind farms [Colour figure can be viewed at wileyonlinelibrary.com]